

Enhanced Energy-Storage Density by Reversible Domain Switching in Acceptor-Doped Ferroelectrics

Zhiyang Wang,¹ Deqing Xue,¹ Yumei Zhou,^{1,*} Nan Wang,¹ Xiangdong Ding,¹ Jun Sun,¹ Turab Lookman², and Dezhen Xue^{1,†}

¹State Key Laboratory for Mechanical Behavior of Materials, Xi'an Jiaotong University, Xi'an 710049, China

²Los Alamos National Laboratory, Los Alamos, New Mexico 87545, USA



(Received 26 October 2020; revised 19 January 2021; accepted 19 February 2021; published 19 March 2021)

By doping and aging in a ferroelectric, we realize a “reversible domain switching” that produces the desirable double hysteresis loop typical of an antiferroelectric with a small remnant polarization and consequently large storage densities. We use Ginzburg-Landau modeling to demonstrate our concept theoretically, and then our predictions are experimentally validated in BaTiO₃-based single crystals (K⁺ doped) and ceramics (Nb⁵⁺ and Mn³⁺ doped), where we measure the enhancement of energy storage due to aging. Based on our experimental results, we estimate that our proposed strategy of doping and aging will result in storage energy density increases of 5 to 35% depending on the ferroelectric system. Thus, our proposed concept can be widely employed across the range of ferroelectric systems. Moreover, as energy dissipation and output efficiency are useful in energy-storage applications, we show how our hybrid doping with acceptor and donor is an efficient way to decrease dissipation and increase output efficiency. In terms of fatigue, we show that even after 10⁶ cycles, the double hysteresis loop of the aged acceptor-doped ferroelectric material yields an energy-storage density and efficiency that is quite robust.

DOI: 10.1103/PhysRevApplied.15.034061

I. INTRODUCTION

Dielectric capacitors, consisting of a dielectric layer between two electrodes, store and release charges and electrical energy through the application and removal of an external electric field [1–3]. They can serve as components in a rechargeable energy-storage system of high-power and pulsed-power applications due to their high electric power output, fast charge-discharge capability, and long cycling lifetimes [4]. However, the low energy densities from dielectric materials limit their applications in compact and efficient electric power systems [5,6]. Hence, there is a critical need to explore new mechanisms that can significantly increase the energy densities of dielectric materials. The stored energy density of a dielectric material (J) is determined by the applied electric field (E) and the electric polarization (P) and is given by

$$J = \int_{P_r}^{P_{\max}} EdP, \quad (1)$$

where the upper limit P_{\max} is the polarization under the maximum electric field, and the lower limit P_r is the remnant polarization (P_r) at zero electric field. Thus, J strongly

depends on P_r , P_{\max} , and E , where the maximum of E is limited by the dielectric breakdown strength (E_b). It is desirable to have a small P_r and large P_{\max} and E_b for electric energy-storage applications [2]. Figures 1(a)–1(c) illustrate the characteristics of three types of dielectric materials used in capacitors that are in common use today. A linear dielectric material responds linearly to the applied electric field according to $P = \epsilon_0 \epsilon_r E$, giving a P_r of 0, as shown in Fig. 1(a). The corresponding J is thus given by $J = \frac{1}{2} \epsilon_0 \epsilon_r E^2$. However, a low value of the relative dielectric constant (ϵ_r) limits the size of the polarization and therefore J . In order to enhance J , many efforts have been devoted to increase the breakdown strength (E_b) by increasing the density, changing the architecture of devices or by optimizing the microstructure [5,7–11].

A ferroelectric material possesses mesoscale size domains with spontaneous polarization, which can be switched along the field direction under an applied electric field. This gives rise to a large P_{\max} . However, the ferroelectric domains often cannot be switched back if the electric field is removed. Consequently, a large remnant polarization (P_r) is obtained, as shown in Fig. 1(c). Thus, by Eq. (1), a ferroelectric material tends to have a low energy-storage density, even though the electric field breakdown strength (E_b) can be moderately large. Antiferroelectric materials are currently the most promising candidates for energy-storage applications [12,13]. In an antiferroelectric,

*zhouyumei@xjtu.edu.cn

†xuedezhen@xjtu.edu.cn

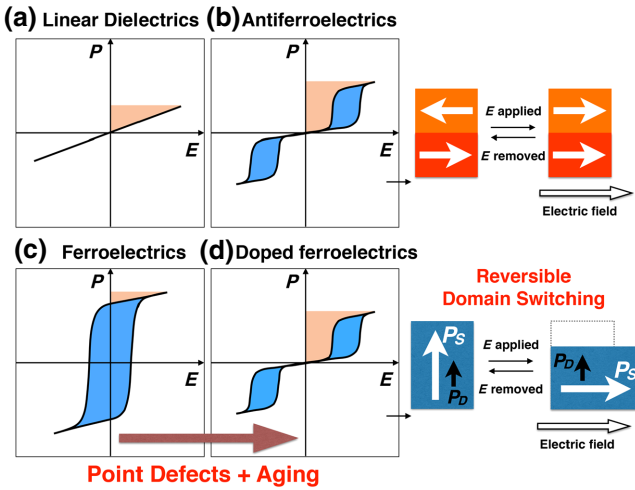


FIG. 1. Schematic illustrations of the polarization as a function of electric field for (a) linear dielectrics; (b) antiferroelectrics; (c) ferroelectrics; (d) acceptor-doped ferroelectrics after aging. The shaded areas in orange and blue are the recoverable energy density and dissipated energy density, respectively. The pinched double hysteresis loops with large spontaneous polarization and small remnant polarization in (b),(d) are favorable for energy storage. The antiparallel arrangement of dipoles in adjacent unit cell in antiferroelectrics is the ground state, which will give rise to the double hysteresis loop, as shown by the schematic beside (b). After acceptor doping and aging treatment, the domain switching in ferroelectrics becomes reversible, giving rise to a pinched double hysteresis loop, as shown by the schematic beside (d).

the electric dipoles align in opposite directions in adjacent unit cells, leading to a net zero polarization. Such an antiferroelectric state can be field induced into a ferroelectric state, and thereby made to exhibit a large net polarization (P_{\max}) under the influence of an electric field. The antialignment is energetically stable and the antiferroelectric state is restored as long as the external electric field is removed, resulting in a near zero P_r , as shown in Fig. 1(b). The double hysteresis loop of Fig. 1(b) allows antiferroelectric materials to provide better energy-storage-density performance than their ferroelectric and linear dielectric counterparts. However, the number of antiferroelectric systems available to date is quite limited and many of them, such as La-doped $\text{Pb}(\text{Zr}, \text{Ti})\text{O}_3$, are Pb-based that introduce their own environmental concerns [12]. In contrast, ferroelectric materials are abundant with many Pb-free systems to choose. Therefore, an alternative strategy, which is the focus of this work, is to start with ferroelectrics but consider how they can be made to have the desired characteristics of antiferroelectrics with a double hysteresis loop. This would then enlarge the possible pool of candidates, especially those without Pb, for acceptable energy-storage densities.

To set the stage for our proposal in this work, we note that in ferroelectrics different domain states are

energetically degenerate and thus there is no driving force to re-establish the initial multidomain state [14]. Consequently, a single-domain state with large remnant polarization P_r always appears after the removal of the field. This inherent irreversibility with regard to domain switching makes it difficult to get potentially large energy storage in ferroelectrics. Here we show that acceptor doping and aging treatment in ferroelectrics can generate an “intrinsic” restoring force to facilitate reversible domain switching so that a small P_r can be obtained without sacrificing P_{\max} . The small P_r and large P_{\max} give rise to an enhanced energy-storage property in ferroelectrics. The acceptor dopants (i.e., ions with valence smaller than the host ions) always generate oxygen vacancies (V_O^-) in the lattice due to charge conservation [15]. These V_O^- are mobile and can redistribute over a long period after a sudden change, such as a structural phase transition or domain reconfiguration [16–18]. In the equilibrium ferroelectric state (i.e., after aging in the ferroelectric state for a long time), the polar crystal symmetry of the ferroelectric phase will lead to a polar distribution of V_O^- . This is supported by electron paramagnetic resonance (EPR) spectroscopy results, which have shown a polar alignment of the cation- V_O^- dipoles (P_d) in acceptor-doped BaTiO_3 [19,20]. Statistically, such a polar alignment creates a net defect polarization $P_D = \sum_{\text{domain}} P_d$ in the same direction as the spontaneous polarization P_s ($P_D \parallel P_s$), and produces an internal bias field [16,21–24]. Thus, within each domain of the multidomain state, the defect polarization P_D and induced internal field stabilize the spontaneous polarization P_s . When such stable domains are switched by an electric field, domain switching occurs abruptly (without diffusion) with P_s following the external electrical field direction. However, the P_D cannot be rotated in such a diffusionless process, since the reorientation of P_D involves the migration of V_O^- [25]. This unswitchable P_D provides a restoring force or reverse internal field favoring a reverse domain switching when the electric field is removed, so a double polarization-electric field (P - E) loop is observed and the remnant polarization P_r is minimized. Therefore, high energy-storage density can be achieved. Such a double hysteresis loop looks similar to that of antiferroelectric materials, but originates from the very different mechanism of reversible domain switching, as shown in Fig. 1(d). In Sec. II we use a Ginzburg-Landau model for BaTiO_3 to predict how a single loop becomes a double loop after aging in a doped system. Moreover, we show how the initial domain pattern of an aged sample can be restored on unloading for the case of the double loop, in contrast to a single loop, and we calculate the energy-storage increase. These predictions are followed by our experimental validation of increases of energy storage due to aging in BaTiO_3 -doped single crystals and ceramics. Based on our experimental results, we estimate that our proposed strategy of doping and aging will result in

storage energy density increases of 5 to 35% depending on the ferroelectric system. Our idea is quite general and applicable to a wide class of ferroelectrics, including thin films, as the phenomena we describe occurs in almost all acceptor-doped ferroelectric materials.

II. MODELING AND EXPERIMENTS

A. Modeling

To give credence to the concept we present above, we first carry out two-dimensional (2D) Ginzburg-Landau simulations in which we introduce a contribution to the Gibbs free energy due to an internal field induced by defects. By evolving the Gibbs free energy as a function of the polarization (\vec{P}), which serves as an order parameter, and the defect field, we can obtain the response of the system to an applied electric field. In particular, we can calculate the polarization-electric field (P - E) hysteresis loop, the evolution of domain patterns under an applied \vec{E} , and the energy-storage density as a function of aging time.

The total free energy, G can be written as the sum of five contributions, including the influence of the internal field (ρ) associated with the defect and aging [26],

$$G = G_L + G_{\text{grad}} + G_{\text{ES}} + G_{\text{EM}} + G_\rho. \quad (2)$$

The term G_L is the Landau expansion of the free energy in terms of (\vec{P}) and is given by

$$\begin{aligned} G_L = & \int \alpha_1(P_x^2 + P_y^2) + \alpha_{11}(P_x^4 + P_y^4) + \alpha_{12}P_x^2P_y^2 \\ & + \alpha_{111}(P_x^6 + P_y^6) + \alpha_{112}(P_x^4P_y^2 + P_x^2P_y^4) \\ & + \alpha_{1111}(P_x^8 + P_y^8) + \alpha_{1112}(P_x^2P_y^6 + P_x^6P_y^2) \\ & + \alpha_{1122}P_x^4P_y^4 - \vec{E} \cdot \vec{P} dv, \end{aligned} \quad (3)$$

where P_x and P_y are the components of the polarization (\vec{P}), and \vec{E} is the external electric field applied to the ferroelectric material. The Ginzburg term G_{grad} is the gradient energy representing the energy to form a domain wall and is given by

$$\begin{aligned} G_{\text{grad}} = & \int \frac{g_1}{2}(P_{x,x}^2 + P_{y,y}^2) \\ & + \frac{g_2}{2}(P_{x,y}^2 + P_{y,x}^2) + g_3 P_{x,x} P_{y,y} dv, \end{aligned} \quad (4)$$

where $P_{i,j}$ represents the partial derivative of P_i ($i = x, y$) with respect to j ($j = x, y$). The term G_{ES} is the electrostatic energy representing the energy contribution of the interaction between depolarization field and dipoles. It can

be written as

$$G_{\text{ES}} = -\frac{1}{2} \int \vec{P} \cdot \vec{E}_d dv, \quad (5)$$

where E_d is the depolarization field originating from the polarization. The term G_{EM} is the electromechanical energy, which describes not only the pure elastic energy but also the coupling between polarization and strain. We define $e_1 = (\epsilon_{xx} + \epsilon_{yy})/\sqrt{2}$, $e_2 = (\epsilon_{xx} - \epsilon_{yy})/\sqrt{2}$ and $e_3 = \epsilon_{xy}$, where the $\epsilon_{i,j}$ are the components of the strain tensor. Then G_{EM} takes the form

$$\begin{aligned} G_{\text{EM}} = & \int \left[\frac{1}{2}A_1 e_1^2 + \frac{1}{2}A_2 e_2^2 + \frac{1}{2}A_3 e_3^2 + \alpha e_1(P_x^2 + P_y^2) \right. \\ & \left. + \beta e_2(P_x^2 - P_y^2) + \gamma e_3 P_x P_y \right] dv. \end{aligned} \quad (6)$$

The above terms are the traditional Ginzburg-Landau free energy. The term G_ρ is the contribution associated with ferroelectric aging due to the defect field, which we assume to be quadratic in ρ with a coupling term $\vec{\rho} \cdot \vec{P}$ so that in equilibrium \vec{P} is determined by ρ . The internal field is not created abruptly that would demand a fourth-order term in ρ . The rationale here is that the point-defect distribution symmetry follows the symmetry of the ferroelectric phase and consequently the defect polarization P_D aligns along the direction of the order parameter \vec{P} [16–18,25]. The G_ρ is given by

$$G_\rho = \int \omega_1(\rho_x^2 + \rho_y^2) - \vec{\rho} \cdot \vec{P} dv, \quad (7)$$

where ρ_x and ρ_y are the components of the internal field vector $\vec{\rho}$, ω_1 is the coefficient that controls the aging process. The kinetics of the domain evolution is described by

$$\frac{\partial P_i}{\partial t} = -\Gamma \frac{\delta G}{\delta P_i}, \quad (8)$$

where Γ is the constant describing the evolution rate. By solving Eq. (8), we are able to obtain P_x and P_y , including their values at a steady state where the right-hand side is close to zero. The distribution of P_x and P_y gives us the equilibrium domain pattern of the ferroelectric system. The evolution of the internal field is governed by the equation,

$$\frac{\partial \rho_i}{\partial t} = -M \frac{\delta G}{\delta \rho_i}, \quad (9)$$

By solving Eq. (9), the values of the internal field at different aging times can be obtained. We thus can calculate the polarization and domain evolution as a function of external electric field at different aging times.

TABLE I. Coefficients of the Ginzburg-Landau free energy and electromechanical energy from Refs. [27,28] (in SI units and T in K).

Coefficient	Values	Unit
α_1	$4.124 \times 10^5(T - 388)$	$C^{-2}m^2N$
α_{11}	4.554×10^8	$C^{-4}m^6N$
α_{12}	8.676×10^8	$C^{-4}m^6N$
α_{111}	1.294×10^9	$C^{-6}m^{10}N$
α_{112}	-1.950×10^9	$C^{-6}m^{10}N$
α_{1111}	3.863×10^{10}	$C^{-8}m^{14}N$
α_{1112}	2.529×10^{10}	$C^{-8}m^{14}N$
g_1	5×10^{-10}	$C^{-2}m^4N$
g_2	2.7×10^{-11}	$C^{-2}m^4N$
g_3	0	$C^{-2}m^4N$
$A1$	2.744×10^{11}	$m^{-2}N$
$A2$	0.816×10^{11}	$m^{-2}N$
$A3$	4.88×10^{11}	$m^{-2}N$
α	-1.281×10^{10}	$C^{-2}m^2N$
β	-0.773×10^{10}	$C^{-2}m^2N$
γ	-1.415×10^{10}	$C^{-2}m^2N$

We utilize BaTiO₃ as a model system, and the coefficients of BaTiO₃ for the traditional Ginzburg-Landau free-energy terms are listed in Table I [27,28]. The parameter $\omega_1 = 8.667 \times 10^{-9} N/V^2$ is chosen so that the magnitude of $|\rho|$ reaches $1.02 \times 10^7 V/m$, comparable to the coercive field. The model is simulated on a 128×128 grid representing a $0.125 \mu m \times 0.125 \mu m$ sample. The two kinetic evolution equations, Eqs. (8) and (9), are solved numerically. As the explicit form of $\delta G/\delta P_i$ only exists in Fourier space, Eq. (8) is solved using a third-order semi-implicit Fourier spectrum method, which allows a faster and more precise solution [29]. Equation (9) is solved using the Euler method, which greatly simplifies the calculation without sacrificing much precision. We note that, at room temperature, domain switching is much faster kinetically than the diffusion of defects, such as V_O^\cdot . Therefore, the rate constant Γ for domain switching is set to be much larger than M for the evolution in ρ . Thus, the internal field ρ can be considered as a constant during the domain-switching process, and we obtain the internal field ρ by solving Eq. (9) based on a stabilized domain configuration. The internal field ρ is then included in the total free energy to obtain the net polarization and microstructure under an external field by solving Eq. (8). The domain configuration and P - E hysteresis loops are then calculated at different aging times (i.e., different values of ρ).

B. Experiments

Experimental validation of our theoretically guided work constitutes a key component of our design strategy. We employ aged and unaged K⁺-doped (Ba, Sr)TiO₃ single crystals and Nb⁵⁺ and Mn³⁺-doped BaTiO₃ ferroelectric ceramics to measure the P - E hysteresis loops.

The as-grown samples are annealed at 1000 °C for 10 h to remove F⁻ so that the remaining K⁺ ions are on the Ba²⁺ site as an acceptor dopant so that oxygen vacancies could be created by charge compensation. The Ba/Sr ratio is analyzed to be about 85/15 and the concentration of K⁺ is determined to be about 1.4 mol% by using an X-ray fluorescence analyzer XRF-1800 from Shimizu Corporation. The Curie temperature of the single crystal, determined by the permittivity versus temperature curves, is about 76 °C. The samples for polarization measurement are coated with silver electrodes on both sides. The ceramic samples are fabricated with a conventional solid-state reaction method using starting chemicals of BaCO₃ (99.95%), Nb₂O₅ (99.9%), Mn₂O₃ (99%), and TiO₂ (99.9%). The starting powder is ball milled for 5 h followed by calcination at 1250 °C for 2 h. The presintered product is milled into powder again and then mixed with PVA as the glue to combine the powder together. The mixture is pressed into pallets under 13 MPa, and then sintered at 1350 °C for 4 h. The aging temperature is set to 80 °C, which is in the ferroelectric state. The ceramic sample for polarization measurement is coated with silver electrodes on both sides. The ferroelectric hysteresis loops are measured with a ferroelectric tester (Radiant Workstation) at 10 Hz, and the fatigue measurements are also conducted on the same tester at 80 Hz under a 30 kV/cm alternating electric field.

III. RESULTS AND DISCUSSION

A. Time-dependent Ginzburg-Landau simulations of the enhancement of energy storage via aging

Figure 2 shows our simulation results for defect-doped BaTiO₃. We simulate the domain switching and polarization change as a function of the electric field for BaTiO₃ before aging ($\rho = 0$). As shown in Fig. 2(a), we start from point ①, a multidomain state with zero net polarization. As the electric field increases, the polarization also increases because domains switch under the influence of the field. At max electric field, a single-domain state is observed where polarization has increased to a maximum (point ② in the P - E curve).

When the electric field is reduced to zero, the single-domain state is preserved and the polarization does not return to zero, giving rise to a remnant polarization (point ③ in the P - E curve). Moreover, applying the electric field in the reverse direction results in another single-domain state (point ④ in the P - E curve) and a normal single hysteresis loop is observed. A high remnant polarization (about 26 $\mu C/cm^2$) we see in Fig. 2(a) gives rise to a low energy-storage density, as indicated by the red shaded area in Fig. 2(a). We next simulate the domain-switching behavior of well-aged BaTiO₃ by applying an electric field to a multidomain state with net polarization of zero, as shown by point ① in the hysteresis loop of

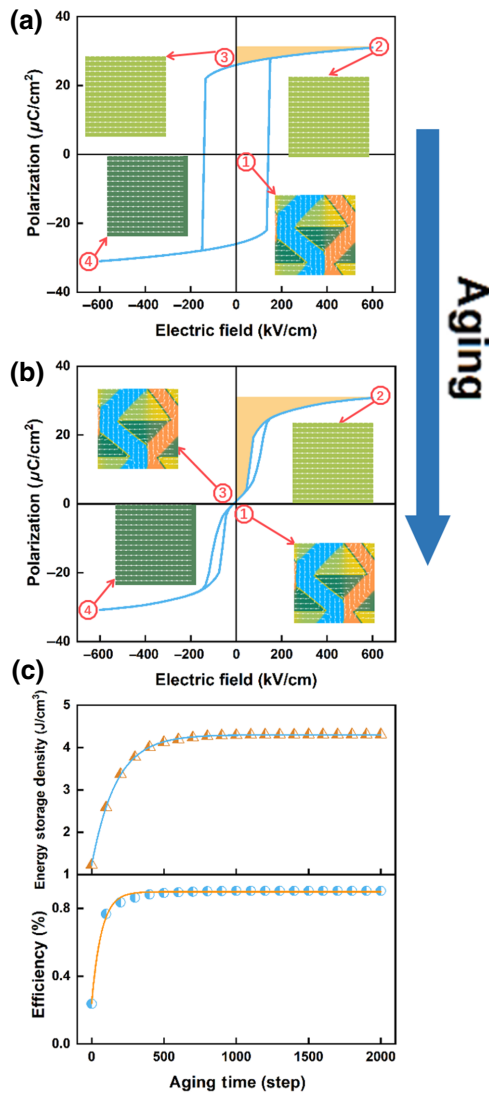


FIG. 2. (a) P - E hysteresis loops from time-dependent Ginzburg-Landau simulations for unaged and aged ferroelectric, respectively. After aging, a single loop turns into a double loop. The insets of (a),(b) are typical domain patterns during loading and unloading. The initial domain pattern of the aged sample in (b) can be restored after unloading, in contrast to that in (a). Both the energy-storage density and the energy efficiency increase with aging time, as shown in (c). The solid line is a guide to the eye.

Fig. 2(b). When the field reaches the maximum, a single-domain configuration is observed, which corresponds to the state of maximum polarization (point ② in the P - E curve). When the electric field is decreased to zero, the same multidomain pattern as the original one is recovered (compare morphologies at points ① and ③) and the net polarization is zero. Furthermore, a similar phenomenon is observed if the electric field direction is reversed except that the polarization assumes a negative value. We thus observe a double P - E hysteresis loop in the aged sample due to reversible domain switching by a cyclic electric

field [17,30]. Of note, the remnant polarization becomes zero, which significantly increases the energy-storage density [the shaded region in Fig. 2(b)]. Figure 2(c) shows the energy-storage density J , calculated from the simulated P - E curve as a function of aging time. Our time scale corresponding to the aging time is represented by the number of time iterations or steps in the numerical simulation of Eq. (9). Both the energy-storage density and efficiency exhibit a gradual increase with time and then saturates. In addition to J , the energy efficiency η , defined as the ratio of recoverable energy density to overall energy input density, is also calculated and is shown as the function of aging time in Fig. 2(c). As the aging-induced reversible domain switching decreases the remanent polarization P_r , η follows the same tendency as J . Thus, we see that aging over an adequate time period facilitates the formation of an internal field by the diffusion of oxygen vacancies (V_O^-), which in turn enhances the energy-storage density as well as the energy efficiency of ferroelectrics.

B. Experimental validation of energy-storage enhancement via aging

We first present our experimental validation of the above theoretical predictions on unaged K^+ -doped $(\text{Ba}, \text{Sr})\text{TiO}_3$ single crystals at room temperature for which we measure the hysteresis loops. The K^+ ions substitute for Ba^{2+} in the perovskite structure of the $(\text{Ba}, \text{Sr})\text{TiO}_3$ crystal and serve as acceptor dopants to generate oxygen vacancies (V_O^-) by charge compensation. We obtain a normal square P - E hysteresis loop as in Fig. 3(a) because there is no defect-induced internal field to facilitate reversible domain switching. The remnant polarization is high ($9.13 \mu\text{C}/\text{cm}^2$) and the corresponding energy density is quite low ($0.022 \text{ J}/\text{cm}^3$). We subsequently aged the K^+ -doped $(\text{Ba}, \text{Sr})\text{TiO}_3$ crystal at room temperature for 324 h and measured its P - E hysteresis loop. As expected, a double hysteresis loop appears, as shown in Fig. 3(b). The remnant polarization P_r drops rapidly to $1.78 \mu\text{C}/\text{cm}^2$ and the corresponding energy-storage density is enhanced to $0.050 \times \text{J}/\text{cm}^3$, as indicated by the shaded region in Fig. 3(b). In addition, the energy efficiency η also increases from 22 to 36%. To find the aging time dependence of J for the single-crystal sample, we proceed to age the sample for different times and calculate J from the corresponding measured P - E loops. In order to ensure the reliability of our experiments, we deage the samples at 200°C for 30 min after each measurement of the hysteresis loop. At 200°C , the ferroelectric phase transforms into the paraelectric phase, and the oxygen vacancies (V_O^-) redistribute randomly at this temperature [25]. We then repeat the process by aging the sample at room temperature for a given time period. The energy-storage density J and efficiency η are plotted as a function of aging time in Fig. 3(c). We

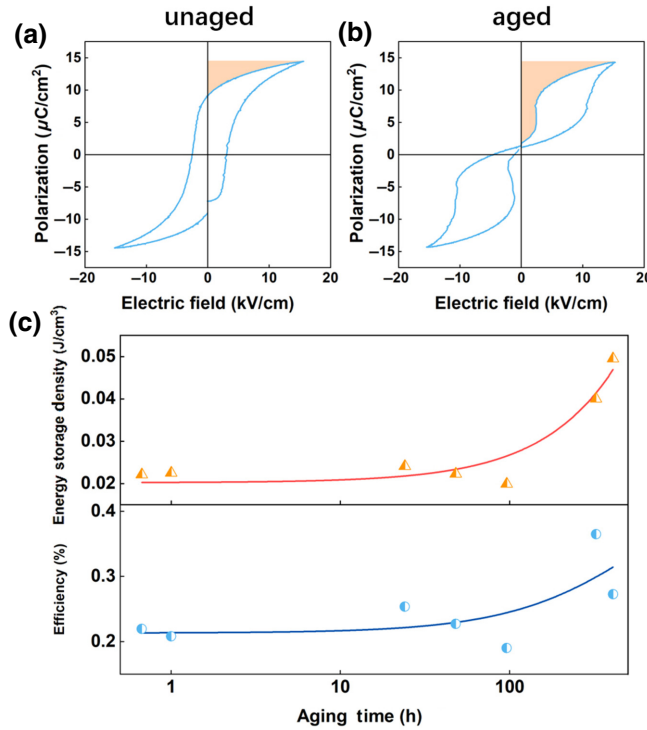


FIG. 3. P - E hysteresis loop for (a) the unaged and (b) aged K⁺-doped strontium barium titanate (BST) single crystal, respectively. The aging time for (b) is 324 h. A single loop transforms a double loop with increasing aging time. (c) The energy-storage density and energy efficiency as a function of aging time. The lines serve as a guide to the eye.

can see that J and η increase with aging time in a similar manner to the simulated result in Fig. 2(c).

We next validate our predictions on ferroelectric ceramics, which are widely used in industrial applications. Our ceramic consisted of a Nb⁵⁺ and Mn³⁺ hybrid-doped in BaTiO₃. The Mn³⁺ ions serve as acceptor dopants, substituting for Ti⁴⁺ so that oxygen vacancies (V_O^{\cdot}) get created by charge compensation. Although Mn manifests with several valence states, such as Mn²⁺, Mn³⁺, and Mn⁴⁺, EPR data shows that the Mn³⁺ ions are dominant in Mn-doped BaTiO₃ ceramics [31–35]. Adding the donor dopants Nb⁵⁺ increases the aging rate and decreases the coercive field, especially the energy dissipation associated with the hysteresis [36–38]. Thus, we expect a more obvious aging effect in this case due to Nb⁵⁺ doping, and hence an enhanced energy efficiency. Figure 4 compares the hysteresis loops for Ba(Ti_{0.99}Mn_{0.01})O_{3- δ} and Ba(Ti_{0.98}Mn_{0.01}Nb_{0.01})O_{3- δ} after aging for 2700 h. The drop in the remnant polarization P_r of the sample with Nb⁵⁺ is more obvious than that for BaTiO₃ without Nb⁵⁺. This suggests that Nb⁵⁺ and Mn³⁺ hybrid-doped BaTiO₃ ceramics give rise to more acute aging effects than Mn³⁺-doped BaTiO₃.

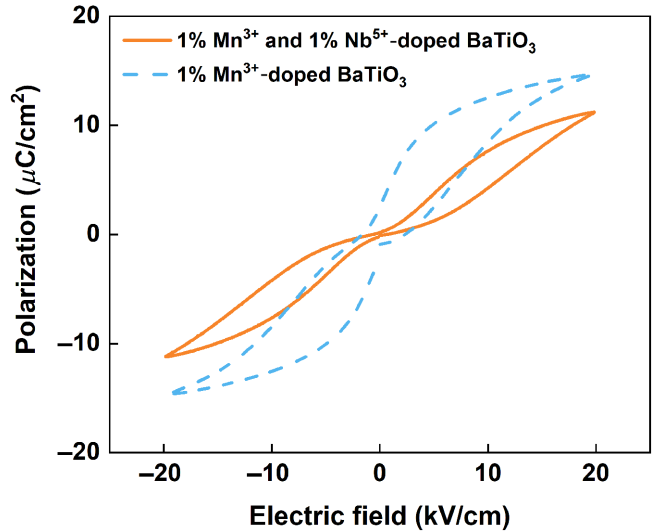


FIG. 4. P - E hysteresis loops for Ba(Ti_{0.99}Mn_{0.01})O_{3- δ} and Ba(Ti_{0.98}Mn_{0.01}Nb_{0.01})O_{3- δ} after aging for 2700 h.

under the same aging time. Moreover, the energy dissipation, the area between the loading and unloading curves, is smaller in Ba(Ti_{0.98}Mn_{0.01}Nb_{0.01})O_{3- δ} compared to Ba(Ti_{0.99}Mn_{0.01})O_{3- δ} . We, therefore, utilize the hybrid-doped BaTiO₃ system for the rest of our measurements. The Curie temperature for the sample, determined from the permittivity versus temperature curves, is about 100 °C. Typical hysteresis loops of unaged and aged samples are shown in Figs. 5(a) and 5(b), respectively. They are similar to the single-crystal sample shown in Figs. 3(a) and 3(b). For the unaged ceramic, a single P - E hysteresis loop is obtained with a small energy-storage density of 0.077 J/cm³ and efficiency of 41%. However, for the aged ceramic, a double P - E hysteresis loop gives rise to a large energy-storage density of 0.150 J/cm³, about twice that of unaged sample. Moreover, the efficiency in the aged sample increases to 73%, and the aging time dependence of the energy-storage density J and the efficiency η are shown in Fig. 5(c). We can see that J and η increase with aging time in a similar manner to the simulated result in Fig. 2(c).

C. Fatigue performance after aging

The stability of the response of the ceramic as a function of the number of cycles with respect to the applied field is crucial for practical energy-storage applications. It determines the fatigue performance of the aged acceptor-doped ferroelectric ceramic, which we study in this section. We apply an alternating electric field of 30 kV/cm to a Ba(Ti_{0.98}Mn_{0.01}Nb_{0.01})O_{3- δ} ceramic sample, which was previously aged for 2700 h. The P - E hysteresis loops of the aged Ba(Ti_{0.98}Mn_{0.01}Nb_{0.01})O_{3- δ} sample for different cycle numbers are shown in Fig. 6(a), where we compare the behavior to unaged Ba(Ti_{0.98}Mn_{0.01}Nb_{0.01})O_{3- δ} . We

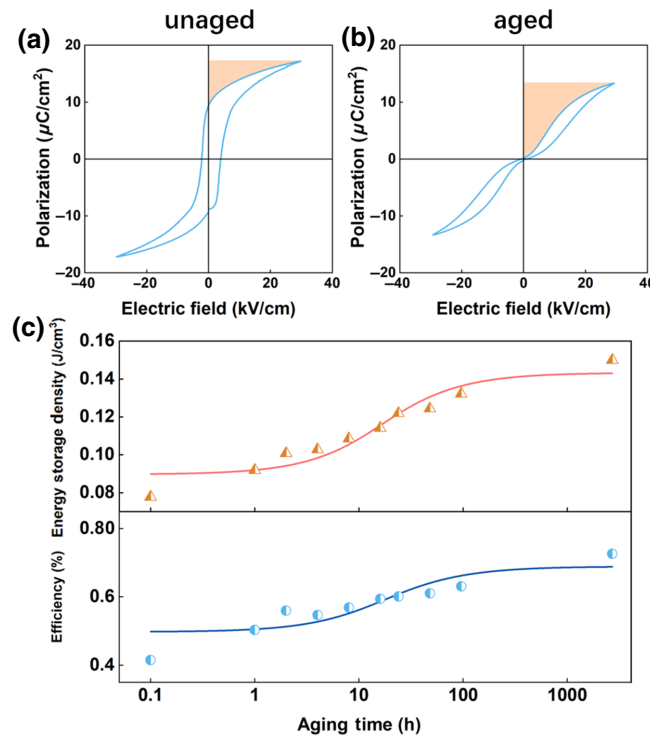


FIG. 5. P - E hysteresis loop for (a) the unaged and (b) aged $\text{Ba}(\text{Ti}_{0.98}\text{Mn}_{0.01}\text{Nb}_{0.01})\text{O}_{3-\delta}$ ceramic, respectively. The shaded areas in (a) and (b) are the recoverable storage energies (J). The aging time for (b) is 2700 h. A single loop transforms to a double loop with increasing aging time. (c) The energy-storage density and efficiency as a function of aging time. The lines serve as a guide to the eye.

observe that the double-loop behavior with higher energy-storage densities persists even after 10^6 cycles. Figure 6(b) shows the energy-storage density and the efficiency as a function of cycling number. The energy-storage density starts to degrade after 10^4 cycles, although the reduction in the energy-storage density is no more than 11% even after 10^6 cycles. It is still appropriately 80% higher than that of the unaged $\text{Ba}(\text{Ti}_{0.98}\text{Mn}_{0.01}\text{Nb}_{0.01})\text{O}_{3-\delta}$ ceramic. The efficiency of the aged $\text{Ba}(\text{Ti}_{0.98}\text{Mn}_{0.01}\text{Nb}_{0.01})\text{O}_{3-\delta}$ ceramic is more robust, decreasing a little from 10^4 to 10^6 cycles. Moreover, we find that during the fatigue measurement, a short break in the electric field cycling allows the ceramic to rejuvenate so that the energy-storage energy recovers. We believe this is because of the hyperfast reaging process, which allows the energy-storage density to recover [39]. Therefore, the enhanced energy-storage density after aging can be potentially used for cycling applications.

In our study, the obtained energy-storage density of the aged BaTiO_3 sample is about 0.15 J/cm^3 , compared to values from $0.1 \sim 0.25 \text{ J/cm}^3$ [40–47] in BaTiO_3 -based systems under the similar electric field range in the literature. The higher values reported are achieved either by fabricating denser and better samples to increase the dielectric breakdown strength, or by doping ions to increase the

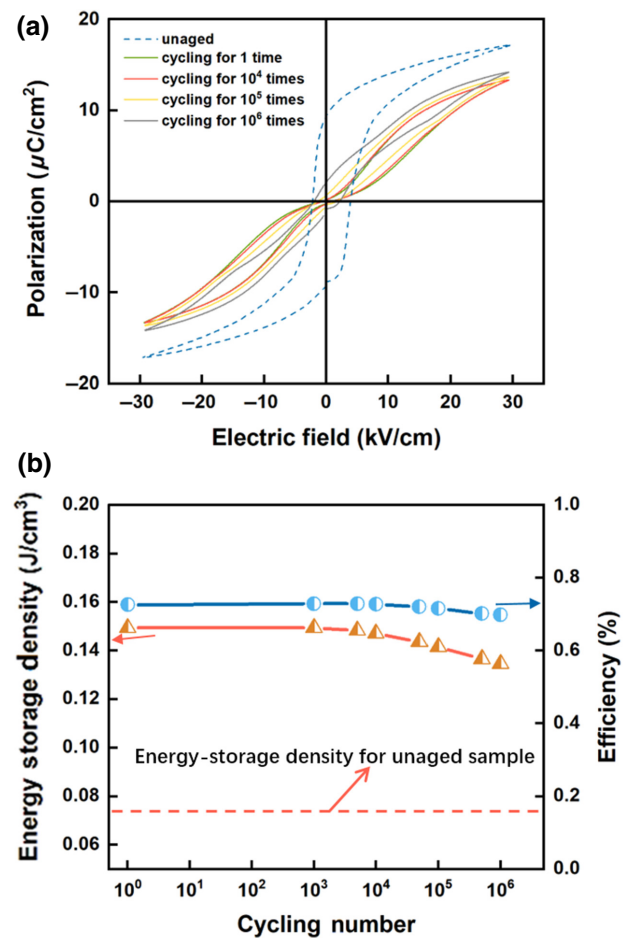


FIG. 6. (a) P - E hysteresis loops for $\text{Ba}(\text{Ti}_{0.98}\text{Mn}_{0.01}\text{Nb}_{0.01})\text{O}_{3-\delta}$ ceramic after cycling for 1, 10^4 , 10^5 , and 10^6 cycles. (b) The energy-storage density and the efficiency as a function of cycle number.

maximum polarization and consequently the permittivity. Our approach of acceptor doping and aging can be further utilized to enhance the energy-storage density of these reported systems *via* changing the single P - E hysteresis loop to a double loop. It should be also noted that the aging treatment may not be applicable to the other two types of dielectrics shown in Figs. 1(a) and 1(b). In antiferroelectrics, the double hysteresis loop persists after aging but with some decay in the maximum polarization [48]. The aging affects only slightly changes the P - E curve of linear and paraelectric materials, however, it can result in a small increase in the dielectric constant [25]. Thus, aging does not have an influence on the energy-storage densities of antiferroelectric, linear materials, compared to ferroelectrics.

IV. CONCLUSIONS

We demonstrate from our predictions using a Ginzburg-Landau model, and subsequent validation experiments on doped single crystal and polycrystalline

ferroelectrics, that energy-storage densities in bulk samples can be enhanced by aging. The acceptor doping generates mobile oxygen vacancies and the aging treatment allows a polar distribution of these mobile defects to induce an internal bias field. This field provides a restoring force for the domains to switch back to their initial domain states to consequently give rise to a double *P-E* hysteresis loop with extremely low remnant polarization. Thus, similar to a double *P-E* hysteresis loop for anti-ferroelectrics, we realize a high energy-storage density in ferroelectrics. There are many acceptor-doped ferroelectric systems, including BiFeO_3 , $\text{K}_{0.5}\text{Na}_{0.5}\text{NbO}_3$, and $\text{Bi}_{0.5}\text{Na}_{0.5}\text{TiO}_3\text{-BaTiO}_3$ [49–51], where a double hysteresis loop and the reversible domain switching can, in general, be realized. Thus our concept can be widely applied across the range of ferroelectric systems. Moreover, as energy dissipation and output efficiency are useful in energy-storage applications, we show how our hybrid doping with acceptor and donor is an efficient way to decrease dissipation and increase output efficiency [36]. In terms of fatigue, we show that even after 10^6 cycles, the double hysteresis loop of the aged acceptor-doped ferroelectric material yields an energy-storage density and efficiency that are quite robust [52]. Our concept is a basis for future improvements in which the choice of ferroelectric system and appropriate hybrid doping can further optimize desired performance. Although we focus on bulk ferroelectrics, our concept can be readily applied and used in thin films, particularly in Pb-free systems, where some of the highest storage energy densities have been measured to date [53]. What is more, the parameters of the phenomenological free energy need to be determined by fitting the results from experiments or simulations. There is considerable scope for the use of molecular simulations and *ab initio* calculations to determine unknown parameters to make the modeling more realistic. For example, the coefficient ω_1 could be determined for BaTiO_3 by REAX calculations, by monitoring the change in polarization due to aging by varying the defect concentration [54,55].

ACKNOWLEDGMENTS

The authors gratefully acknowledge the support of National Natural Science Foundation of China (Grants No. 51671157, No. 51571156, and No. 51931004), (2017YFB0702401) and the 111 project 2.0 (BP2018008). We thank the anonymous reviewer for the highly constructive comments. T.L. thanks LANL where the work was carried out.

[1] B. Chu, X. Zhou, K. Ren, B. Neese, M. Lin, Q. Wang, F. Bauer, and Q. M. Zhang, A dielectric polymer with high electric energy density and fast discharge speed, *Science* **313**, 334 (2006).

- [2] L. Yang, X. Kong, F. Li, H. Hao, Z. Cheng, H. Liu, J.-F. Li, and S. Zhang, Perovskite lead-free dielectrics for energy storage applications, *Prog. Mater. Sci.* **102**, 72 (2019).
- [3] H. Pan, F. Li, Y. Liu, Q. Zhang, M. Wang, S. Lan, Y. Zheng, J. Ma, L. Gu, Y. Shen, P. Yu, S. Zhang, L.-Q. Chen, Y.-H. Lin, and C.-W. Nan, Ultrahigh-energy density lead-free dielectric films via polymorphic nanodomain design, *Science* **365**, 578 (2019).
- [4] H. Huang and J. Scott, *Ferroelectric Materials for Energy Applications* (Wiley, Weinheim, German, 2019).
- [5] Y. Wang, J. Cui, Q. Yuan, Y. Niu, Y. Bai, and H. Wang, Significantly enhanced breakdown strength and energy density in sandwich-structured barium titanate/poly(vinylidene fluoride) nanocomposites, *Adv. Mater.* **27**, 6658 (2015).
- [6] Z.-M. Dang, J.-K. Yuan, S.-H. Yao, and R.-J. Liao, Flexible nanodielectric materials with high permittivity for power energy storage, *Adv. Mater.* **25**, 6334 (2013).
- [7] Y. Song, Y. Shen, H. Liu, Y. Lin, M. Li, and C.-W. Nan, Improving the dielectric constants and breakdown strength of polymer composites: Effects of the shape of the BaTiO_3 nanoinclusions, surface modification and polymer matrix, *J. Mater. Chem.* **22**, 16491 (2012).
- [8] Q. Li, G. Zhang, F. Liu, K. Han, M. R. Gadinski, C. Xiong, and Q. Wang, Solution-processed ferroelectric terpolymer nanocomposites with high breakdown strength and energy density utilizing boron nitride nanosheets, *Energy Environ. Sci.* **8**, 922 (2015).
- [9] Y. Wang, J. Cui, L. Wang, Q. Yuan, Y. Niu, J. Chen, Q. Wang, and H. Wang, Compositional tailoring effect on electric field distribution for significantly enhanced breakdown strength and restrained conductive loss in sandwich-structured ceramic/polymer nanocomposites, *J. Mater. Chem. A* **5**, 4710 (2017).
- [10] J. Yin, Y. Zhang, X. Lv, and J. Wu, Ultrahigh energy-storage potential under low electric field in bismuth sodium titanate-based perovskite ferroelectrics, *J. Mater. Chem. A* **6**, 9823 (2018).
- [11] Z. Cai, C. Zhu, H. Wang, P. Zhao, Y. Yu, L. Li, and X. Wang, Giant dielectric breakdown strength together with ultrahigh energy density in ferroelectric bulk ceramics via layer-by-layer engineering, *J. Mater. Chem. A* **7**, 17283 (2019).
- [12] X. Hao, J. Zhai, L. B. Kong, and Z. Xu, A comprehensive review on the progress of lead zirconate-based antiferroelectric materials, *Prog. Mater. Sci.* **63**, 1 (2014).
- [13] B. Xu, J. Íñiguez, and L. Bellaiche, Designing lead-free antiferroelectrics for energy storage, *Nat. Commun.* **8**, 15682 (2017).
- [14] M. Lines and A. Glass, *Principles and Applications of Ferroelectrics and Related Materials*, International Series of Monographs on Physics (OUP Oxford, Oxford, England, 2001).
- [15] D. Smyth, *The Defect Chemistry of Metal Oxides*, Classic Dielectric Science Book Series (Oxford University Press, Oxford, England, 2000).
- [16] X. Ren, Large electric-field-induced strain in ferroelectric crystals by point-defect-mediated reversible domain switching, *Nat. Mater.* **3**, 91 (2004).

- [17] L. X. Zhang and X. Ren, In situ observation of reversible domain switching in aged Mn-doped BaTiO₃ single crystals, *Phys. Rev. B* **71**, 174108 (2005).
- [18] D. Xue, J. Gao, H. Bao, Y. Zhou, L. Zhang, and X. Ren, In situobservation of thermally activated domain memory and polarization memory in an aged K⁺-doped (Ba, Sr)TiO₃ single crystal, *J. Phys.: Condens. Matter* **23**, 275902 (2011).
- [19] L. Zhang, E. Erdem, X. Ren, and R.-A. Eichel, Reorientation of (Mn[”]_{Ti} – V^{••}_O) defect dipoles in acceptor-modified BaTiO₃ single crystals: An electron paramagnetic resonance study, *Appl. Phys. Lett.* **93**, 202901 (2008).
- [20] E. Erdem, P. Jakes, R.-A. Eichel, D. C. Sinclair, M. Pasha, and I. M. Reaney, Formation of (Ti[']_{Ti} – V^{••}_O)[•] defect dipoles in BaTiO₃ ceramics heat-treated under reduced oxygen partial-pressure, *Funct. Mater. Lett.* **03**, 65 (2010).
- [21] Y. Zhou, D. Xue, X. Ding, L. Zhang, J. Sun, and X. Ren, Modeling the paraelectric aging effect in the acceptor doped perovskite ferroelectrics: Role of oxygen vacancy, *J. Phys.: Condens. Matter* **25**, 435901 (2013).
- [22] W. Warren, D. Dimos, G. Pike, K. Vanheusden, and R. Ramesh, Alignment of defect dipoles in polycrystalline ferroelectrics, *Appl. Phys. Lett.* **67**, 1689 (1995).
- [23] W. Warren, G. Pike, K. Vanheusden, D. Dimos, B. Tuttle, and J. Robertson, Defect-dipole alignment and tetragonal strain in ferroelectrics, *J. Appl. Phys.* **79**, 9250 (1996).
- [24] R. Lohkämper, H. Neumann, and G. Arlt, Internal bias in acceptor-doped BaTiO₃ ceramics: Numerical evaluation of increase and decrease, *J. Appl. Phys.* **68**, 4220 (1990).
- [25] D. Xue, J. Gao, L. Zhang, H. Bao, W. Liu, C. Zhou, and X. Ren, Aging effect in paraelectric state of ferroelectrics: Implication for a microscopic explanation of ferroelectric deaging, *Appl. Phys. Lett.* **94**, 082902 (2009).
- [26] D. Xue, Y. Zhou, X. Ding, T. Lookman, J. Sun, and X. Ren, Aging and deaging effects in shape memory alloys, *Phys. Rev. B* **86**, 184109 (2012).
- [27] Y. L. Li, L. E. Cross, and L. Q. Chen, A phenomenological thermodynamic potential for BaTiO₃ single crystals, *J. Appl. Phys.* **98**, 064101 (2005).
- [28] M. Porta, T. Lookman, and A. Saxena, Effects of criticality and disorder on piezoelectric properties of ferroelectrics, *J. Phys.: Condens. Matter* **22**, 345902 (2010).
- [29] H.-L. Hu and L.-Q. Chen, Three-dimensional computer simulation of ferroelectric domain formation, *J. Am. Ceram. Soc.* **81**, 492 (1998).
- [30] L. Zhang and X. Ren, Aging behavior in single-domain Mn-doped BaTiO₃ crystals: Implication for a unified microscopic explanation of ferroelectric aging, *Phys. Rev. B* **73**, 094121 (2006).
- [31] H. T. Langhammer, T. Müller, K.-H. Felgner, and H.-P. Abicht, Crystal structure and related properties of manganese-doped barium titanate ceramics, *J. Am. Ceram. Soc.* **83**, 605 (2000).
- [32] T. Kutty and P. Murugaraj, Epr study on the role of mn in enhancing ptc of BaTiO₃, *Mater. Lett.* **3**, 195 (1985).
- [33] P. Lambeck and G. Jonker, The nature of domain stabilization in ferroelectric perovskites, *J. Phys. Chem. Solids* **47**, 453 (1986).
- [34] M. Nakahara and T. Murakami, Electronic states of Mn ions in Ba_{0.97}Sr_{0.03}TiO₃ single crystals, *J. Appl. Phys.* **45**, 3795 (1974).
- [35] S. Desu and E. Subbarao, Effect of oxidation states of mn on the phase stability of Mn-doped BaTiO₃, *Ferroelectrics* **37**, 665 (1981).
- [36] W. Liu, W. Chen, L. Yang, L. Zhang, Y. Wang, C. Zhou, S. Li, and X. Ren, Ferroelectric aging effect in hybrid-doped BaTiO₃ ceramics and the associated large recoverable electrostrain, *Appl. Phys. Lett.* **89**, 172908 (2006).
- [37] H. Bao, J. Gao, D. Xue, C. Zhou, L. Zhang, W. Liu, and X. Ren, Control of ferroelectric aging by manipulating point defects, *Ferroelectrics* **401**, 45 (2010).
- [38] C. Zhou, W. Liu, H. Bao, J. Gao, D. Xue, and X. Ren, Aging effect in acceptor-donor co-doped ferroelectrics, *Ferroelectrics* **404**, 141 (2010).
- [39] See Supplemental Material at <http://link.aps.org/supplemental/10.1103/PhysRevApplied.15.034061> for the hyper-fast reaging process.
- [40] H. Ogihara, C. A. Randall, and S. Trolier-McKinstry, High-energy density capacitors utilizing 0.7 BaTiO₃–0.3 BiScO₃ ceramics, *J. Am. Ceram. Soc.* **92**, 1719 (2009).
- [41] W.-B. Li, D. Zhou, L.-X. Pang, R. Xu, and H.-H. Guo, Novel barium titanate based capacitors with high energy density and fast discharge performance, *J. Mater. Chem. A* **5**, 19607 (2017).
- [42] Z. Shen, X. Wang, B. Luo, and L. Li, BaTiO₃–BiYbO₃ perovskite materials for energy storage applications, *J. Mater. Chem. A* **3**, 18146 (2015).
- [43] V. S. Puli, D. K. Pradhan, D. B. Chrisey, M. Tomozawa, G. Sharma, J. Scott, and R. S. Katiyar, Structure, dielectric, ferroelectric, and energy density properties of (1 – x) BZT–xBCT ceramic capacitors for energy storage applications, *J. Mater. Sci.* **48**, 2151 (2013).
- [44] X. Wang, Y. Zhang, X. Song, Z. Yuan, T. Ma, Q. Zhang, C. Deng, and T. Liang, Glass additive in barium titanate ceramics and its influence on electrical breakdown strength in relation with energy storage properties, *J. Eur. Ceram. Soc.* **32**, 559 (2012).
- [45] R. Yuan, Y. Tian, D. Xue, D. Xue, Y. Zhou, X. Ding, J. Sun, and T. Lookman, Accelerated search for BaTiO₃-based ceramics with large energy storage at low fields using machine learning and experimental design, *Adv. Sci.* **6**, 1901395 (2019).
- [46] T. Wang, L. Jin, C. Li, Q. Hu, and X. Wei, Relaxor ferroelectric BaTiO₃–Bi (Mg_{2/3}Nb_{1/3})O₃ ceramics for energy storage application, *J. Am. Ceram. Soc.* **98**, 559 (2015).
- [47] Q. Hu, L. Jin, T. Wang, C. Li, Z. Xing, and X. Wei, Dielectric and temperature stable energy storage properties of 0.88 BaTiO₃–0.12 Bi (Mg_{1/2}Ti_{1/2})O₃ bulk ceramics, *J. Alloys Compd.* **640**, 416 (2015).
- [48] X. Tan, Z. Xu, X. Liu, and Z. Fan, Double hysteresis loops at room temperature in NaNbO₃-based lead-free antiferroelectric ceramics, *Mater. Res. Lett.* **6**, 159 (2018).
- [49] G. L. Yuan, Y. Yang, and S. W. Or, Aging-induced double ferroelectric hysteresis loops in BiFeO₃ multiferroic ceramic, *Appl. Phys. Lett.* **91**, 122907 (2007).
- [50] Z. Feng and X. Ren, Striking similarity of ferroelectric aging effect in tetragonal, orthorhombic and rhombohedral crystal structures, *Phys. Rev. B* **77**, 134115 (2008).
- [51] W. Jo, E. Erdem, R.-A. Eichel, J. Glaum, T. Granzow, D. Damjanovic, and J. Rödel, Effect of Nb-donor and Fe-acceptor dopants in (Bi_{1/2}Na_{1/2})TiO₃–BaTiO₃–(K_{0.5}Na_{0.5})

- NbO₃ lead-free piezoceramics, *J. Appl. Phys.* **108**, 014110 (2010).
- [52] L. X. Zhang, W. Chen, and X. Ren, Large recoverable electrostrain in Mn-doped (Ba, Sr)TiO₃ ceramics, *Appl. Phys. Lett.* **85**, 5658 (2004).
- [53] H. Pan, J. Ma, J. Ma, Q. Zhang, X. Liu, B. Guan, L. Gu, X. Zhang, Y.-J. Zhang, L. Li, and et al, Giant energy density and high efficiency achieved in bismuth ferrite-based film capacitors via domain engineering, *Nat. Commun.* **9**, 1 (2018).
- [54] D. Akbarian, D. E. Yilmaz, Y. Cao, P. Ganesh, I. Dabo, J. Munro, R. Van Ginhoven, and A. C. van Duin, Understanding the influence of defects and surface chemistry on ferroelectric switching: A reaxff investigation of BaTiO₃, *Phys. Chem. Chem. Phys.* **21**, 18240 (2019).
- [55] K. Kelley, D. Yilmaz, L. Collins, Y. Sharma, H. Lee, D. Akbarian, A. Van Duin, P. Ganesh, and R. Vasudevan, Thickness and strain dependence of piezoelectric coefficient in BaTiO₃ thin films, *Phys. Rev. Mater.* **4**, 024407 (2020).